BIOCHEMISTRY

 Volume 44, Number 4 February 1, 2005

Accelerated Publications

Intramolecular Occlusion of the Diacylglycerol-Binding Site in the C_1 Domain of Munc13-1[†,‡]

Nan Shen, Oleg Guryev, and Josep Rizo*

Departments of Biochemistry and Pharmacology, University of Texas Southwestern Medical Center, 5323 Harry Hines Boulevard, Dallas, Texas 75390

Received November 11, 2004; Revised Manuscript Received December 12, 2004

ABSTRACT: Protein kinase C (PKC) isozymes and other receptors of diacylglycerol (DAG) bind to this widespread second messenger through their C_1 domains. These alternative DAG receptors include munc13-1, a large neuronal protein that is crucial for DAG-dependent augmentation of neurotransmitter release. Whereas the structures of several PKC C_1 domains have been determined and have been shown to require little conformational changes for ligand binding, it is unclear whether the C_1 domains from other DAG receptors contain specific structural features with key functional significance. To gain insight into this question, we have determined the three-dimensional structure in solution of the munc13-1 C_1 domain using NMR spectroscopy. The overall structure includes two β-sheets, a short C-terminal α-helix, and two Zn^{2+}-binding sites, resembling the structures of PKC C_1 domains. However, the munc13-1 C_1 domain exhibits striking structural differences with the PKC C_1 domains in the ligand-binding site. These differences result in occlusion of the binding site of the munc13-1 C_1 domain by a conserved tryptophan side chain that in PKCs adopts a completely different orientation. As a consequence, the munc13-1 C_1 domain requires a considerable conformational change for ligand binding. This structural distinction is expected to decrease the DAG affinity of munc13-1 compared to that of PKCs, and is likely to be critical for munc13-1 function. On the basis of these results, we propose that augmentation of neurotransmitter release may be activated at higher DAG levels than PKCs as a potential mechanism for uncoupling augmentation of release from the multitude of other signaling processes mediated by DAG.

Diacylglycerol (DAG)[1] acts as a second messenger in multiple signal transduction pathways that are activated by diverse extracellular stimuli, regulating a wide variety of cellular functions that range from cell proliferation, differentiation, and apoptosis to modulation of neurotransmitter release and hormone secretion. The different isoforms of protein kinase C (PKC) were traditionally believed to be the targets of DAG and of phorbol esters (PEs), strong tumor-promoting agents from the plant family Euphorbiaceae that mimic the actions of DAG (*1*, *2*). However, the identification of several protein families that also bind DAG and PEs has suggested a high degree of complexity in the signaling pathways activated by DAG (reviewed in refs *3*−*5*). Thus, although PKCs are undoubtedly major targets of DAG signaling, it is now clear that other DAG receptors mediate

[†] This work was supported by NIH Grant NS37200 to J.R.

[‡] Structures have been deposited in the RCSB Protein Data Bank (entry 1Y8F).

* To whom correspondence should be addressed. Phone: (214) 648-9026. Fax: (214) 648-8673. E-mail: jose@arnie.swmed.edu.

[1] Abbreviations: DAG, diacylglycerol; DOG, dioctanoylglycerol; PKC, protein kinase C; GRP, Rac GTPase activating protein; PE, phorbol ester.

10.1021/bi0476127 CCC: $30.25
Published on Web 12/31/2004

certain key regulatory processes that had initially been attributed to PKCs. However, little is known about how the different DAG receptors discriminate among distinct DAG-mediated signals.

Well-established "non-PKC" receptors of DAG are the members of the unc13/munc13 family of neuronal proteins (reviewed in ref *6*). The functional importance of these large (ca. 200 kDa) multidomain proteins has been demonstrated by the complete block in neurotransmitter release caused by double knockout in mice of the two major isoforms, munc13-1 and munc13-2, as well as by deletion of unc13 in invertebrates (*7*−*10*). In addition to an essential function in release, unc13/munc13s are believed to play critical roles in activity-dependent changes in the efficacy of release that likely underlie some forms of information processing in the nervous system. In particular, genetic experiments have shown that facilitation of release at the neuromuscular junction in *Caenorhabditis elegans* by DAG depends on unc13 (*11*), and that munc13-1 is the major DAG receptor that mediates DAG-induced augmentation of release in mammalian hippocampal neurons (*12*). The critical importance of this function is emphasized by the lethal phenotype caused by mutations that disrupt DAG binding to munc13-1 (*12*).

All DAG/PE receptors share a small cysteine-rich domain that is responsible for ligand binding and is known as the C_1 domain (*13*). Ligand binding to the C_1 domain induces or contributes to protein translocation to the membrane, leading to receptor activation. Whereas some DAG receptors contain a single C_1 domain (e.g., unc13/munc13s), PKCs contain tandem C_1 domains (termed C_1A and C_1B domains). The solution structure of the PKCα C_1B domain determined by NMR spectroscopy showed that C_1 domains contain two β-sheets and a short C-terminal α-helix, and coordinate two zinc ions via two similar motifs (*14*). Each of these motifs is formed by three cysteines and one histidine that are distant in the sequence, which distinguishes C_1 domains from classical "zinc fingers". The crystal structure of the PKCδ C_1B domain in the absence and presence of phorbol 13-acetate later revealed an analogous architecture, and showed that the ligand binds at a groove between two loops at one tip of the domain (*15*). The apo and holo structures of the domain were practically identical, showing that ligand binding does not require substantial conformational changes. However, PE binding results in a continuous hydrophobic surface that covers one-third of the domain, which probably underlies how ligand binding promotes insertion of the domain into the membrane (*15*). The structures of the C_1 domains from KSR and Raf-1, which do not bind DAG/PE (*16*, *17*), and of the PKCγ C_1B domain (*18*) have provided additional information about the structural diversity within the C_1 domain family, but no three-dimensional structural information is available on C_1 domains from non-PKC targets of DAG signaling. It is thus unclear whether the C_1 domains of these alternative DAG receptors contain specific structural features that may underlie fundamental functional distinctions, perhaps discriminating between different types of DAG-mediated signals.

To gain insight into this question and into the structural basis for DAG-induced augmentation of neurotransmitter release, we have determined the three-dimensional structure in solution of the munc13-1 C_1 domain using multidimensional NMR spectroscopy. We find that the overall conformation of the munc13-1 C_1 domain is analogous to that of the PKCδ C_1B domain, but the ligand-binding region exhibits striking structural differences. Importantly, a conserved tryptophan residue occludes the DAG/PE-binding site in the munc13-1 C_1 domain. Hence, unlike the PKCδ C_1B domain, the munc13-1 C_1 domain needs to experience a considerable conformational change for ligand binding. These results suggest that DAG-dependent augmentation of neurotransmitter release may require DAG levels higher than those involved in PKC activation, and that intramolecular inhibition of ligand binding in some C_1 domains may provide a mechanism for discriminating among distinct DAG-dependent cellular signals.

EXPERIMENTAL PROCEDURES

Protein Expression and Purification. A construct for expression of the rat munc13-1 C_1 domain (residues 567−616) as a GST fusion protein was generated from a cDNA containing the entire rat munc13-1 sequence (*19*) by PCR using custom-designed primers, and subcloned into pGEX-KG (*20*). This expression vector was used to generate a construct for expression of the W588 mutant munc13-1 C_1 domain, also using PCR and custom-designed primers. Uniformly ^{15}N- or ^{15}N- and ^{13}C-labeled samples of the wild-type or W588A mutant munc13-1 C_1 domain were expressed in bacteria grown in minimal media supplemented with ^{15}-NH_4Cl and with or without [$^{13}C_6$]glucose (CIL, Andover, MA) as the sole nitrogen and carbon sources, respectively. The fusion protein was affinity-purified on glutathione−Sepharose (Pharmacia), cleaved from the GST moiety with thrombin (Sigma), and purified by gel filtration in buffer A [40 mM HEPES (pH 7.0), 150 mM NaCl, and 50 μM $ZnCl_2$].

NMR Spectroscopy. All NMR experiments were carried out at 25 °C on a Varian Inova600 spectrometer. ^{1}H−^{15}N HSQC spectra for DOG binding studies were acquired on 100 μM samples of the wild-type or W588A mutant munc13-1 C_1 domain dissolved in buffer A containing 20 mM CHAPS in the absence or presence of 0.7 mM DOG (under these conditions, DOG is fully incorporated into the CHAPS micelles as judged by ^{1}H NMR spectroscopy). One uniformly ^{15}N-labeled sample and one uniformly ^{15}N- and ^{13}C-labeled sample of the wild-type munc13-1 C_1 domain (1.5 mM) dissolved in buffer A were used for structure determination, which was accomplished using a suite of pulsed-field gradient-enhanced NMR experiments (*21*−*23*). Briefly, these included two-dimensional ^{1}H−^{13}C CT-HSQC and three-dimensional (3D) ^{1}H−^{15}N TOCSY-HSQC, HNCO, HNCACB, CBCA(CO)NH, (H)C(CO)NH-TOCSY, H(C)-(CO)NH-TOCSY, HCCH-TOCSY, ^{1}H−^{15}N NOESY-HSQC, and ^{1}H−^{13}C NOESY-HSQC spectra (150 ms mixing time for the NOESY spectra). Protection of amide protons from the solvent was assessed from the intensities of exchange cross-peaks with the water resonance in 3D ^{1}H−^{15}N TOCSY-HSQC experiments. Stereospecific assignments of Val and Leu methyl groups were obtained from examination of NOE patterns in combination with χ_1 and χ_2 angles derived from a 3D ^{13}C−^{13}C long-range correlation spectrum (*24*). All data were processed with NmrPipe (*25*) and analyzed with NMRview (*26*).

For structure calculations, NOE cross-peak intensities were classified as strong, medium, weak, and very weak, and

assigned to restraints of 1.8−2.8, 1.8−3.5, 1.8−5.0, and 1.8−6.0 Å, respectively, with appropriate pseudoatom corrections. ϕ and ψ torsion angle restraints were included on the basis of the analysis of HN, ^{15}N, ^{13}Cα, ^{13}CO, and ^{13}Cβ chemical shifts using TALOS (*27*). Dihedral angles were restrained to the maximum of 22.5° or 1.5 times the standard deviation observed in the TALOS database matches. Restraints to ensure the proper geometry of the two Zn^{2+}-binding sites were incorporated at the final stages of the calculations. These restraints were derived from the Zn^{2+}−ligand and ligand−ligand distances observed in the crystals structures of the PKCδ C_1B domain and the Zn^{2+}-binding domain of DNA primase (PDB entries 1PTQ and 1D0Q, respectively), where the Zn^{2+} ions are also coordinated by three cysteine side chains and one histidine side chain. On the basis of this analysis, the Zn^{2+} ions were covalently attached to ND1 of the histidine side chains (2.3 Å bond length), and Zn^{2+}−S, S−S, and S−ND1 distances were restrained to 2.3−2.5, 3.7−4.2, and 3.6−4.1 Å, respectively. Hydrogen bond restraints of 1.3−2.5 and 2.3−3.5 Å were used for H−O and N−O distances, respectively. Structures of the munc13-1 C_1 domain were calculated using torsion angle-simulated annealing with CNS (*28*). A total of 2000 structures were calculated with the final set of restraints, and the 20 structures with the lowest NOE energies were selected.

RESULTS

Structure of the munc13-1 C_1 Domain. To determine the three-dimensional structure in solution of the munc13-1 C_1 domain, we first assigned its ^{1}H, ^{15}N, and ^{13}C resonances using standard triple-resonance experiments. The excellent chemical shift dispersion of this small domain allowed us to assign all backbone and side chain resonances, with the exception of three backbone NH groups from the predicted ligand-binding loops (T575, G589, and I590) that were broadened beyond detection because of chemical exchange. However, we were able to assign all the CH resonances from these three residues on the basis of HCCH-TOCSY data and unambiguous NOEs observed in a 3D ^{1}H−^{13}C NOESY-HSQC experiment. Preliminary analysis of NOE patterns revealed that the munc13-1 C_1 domain has the expected secondary structure based on sequence homology with the PKCδ C_1B domain. However, the NOE patterns also indicated substantial structural differences in the predicted ligand-binding loops. In particular, we observed numerous unexpected NOEs involving the aromatic protons of W588 (e.g., those illustrated in Figure 1), which suggested that this conserved side chain adopts an orientation completely different from that observed in the PKCδ C_1B domain.

Preliminary structure calculations with unambiguous NOE data confirmed that the side chains from the two Zn^{2+}-binding motifs, each composed of three cysteines and one histidine, were properly oriented for metal coordination, and structure refinement was performed with restraints to ensure the proper geometry of the Zn^{2+}-binding sites. Final structure calculations were performed using these restraints together with 861 experimental restraints that included 384 long-range NOEs. Figure 2A shows a stereodiagram of a backbone superposition of the 20 structures with the lowest NOE energies, and a ribbon diagram of a representative structure is shown in Figure 2B. The structural statistics are summarized in Table 1. As expected, the munc13-1 C_1 domain

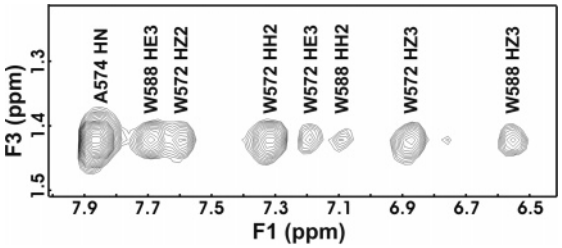

FIGURE 1: Unexpected NOEs involving the W588 side chain of the munc13-1 C_1 domain. The diagram shows a contour plot of an expansion from an (F1,F3) plane of a 3D ^{1}H−^{13}C NOESY-HSQC spectrum of the munc13-1 C_1 domain, corresponding to the ^{13}C chemical shift of the A574 βCH$_3$ group (20.0 ppm). The assignments of the NOEs are given. NOEs with the W588 aromatic protons were unexpected on the basis of the crystal structure of the PKCδ C_1B domain.

contains two antiparallel β-sheets with a total of five β-strands (labeled β1−β5 in Figure 2), and a short C-terminal α-helix. The predicted ligand-binding loops emerge at the top of the domain in the orientation shown in Figure 2 (labeled loop 1 and loop 2). The structure is well-defined throughout most of the domain, with backbone rms deviations of 0.38 Å for the whole domain and 0.14 Å for the elements of secondary structure. The quality of the structure is also illustrated by low deviations from the experimental restraints and from idealized covalent geometry (Table 1). The small percentage of residues in the nonallowed regions of the Ramachandran map corresponds to I590 in loop 2 of a subset of structures, and can be attributed to a paucity of NOE data in this region of the domain that probably also underlies the lack of structural definition in part of this loop (see Figure 2). However, some conformational averaging likely exists in this region, as manifested by the resonance broadening that prevented observation of some NH groups.

W588 Occludes the DAG Binding Site in the munc13-1 C_1 Domain. Structural comparisons using DALI (*29*) revealed that, as expected, the structure of the munc13-1 C_1 domain most closely resembles those of the PKC C_1 domains among the structures available in the Protein Data Bank (PDB), being most similar to the PKCδ C_1B domain. The munc13-1 C_1 domain and PKCδ C_1B domain structures are indeed very similar throughout most of the domain, as illustrated by the backbone superposition shown in Figure 3A, but a conspicuous difference is observed in the conformation of one of the ligand-binding loops (loop 2). In fact, the trace rms deviation between the entire domains, 1.7 Å for 50 equivalent Cα atoms, decreases to 0.8 Å for 39 equivalent Cα atoms when loop 2 and a few somewhat disordered residues in the termini are not included in the superposition. These results apply to comparisons using the structures of the PKCδ C_1B domain in the absence or presence of phorbol 13-acetate since they are practically identical [the trace rms deviation of 0.28 between the two structures is probably within experimental error (*15*)].

Superposition of a representative structure of the munc13-1 C_1 domain with that of the phorbol 13-acetate-bound PKCδ C_1B domain (Figure 3B) revealed a key consequence of the different conformation of loop 2 in the two C_1 domains that was already indicated by our preliminary analysis of the NOE data: the side chain of W588 of the munc13-1 C_1 domain, whose location is well-defined despite some structural heterogeneity in loop 2 (see Figure 2A), adopts an orientation

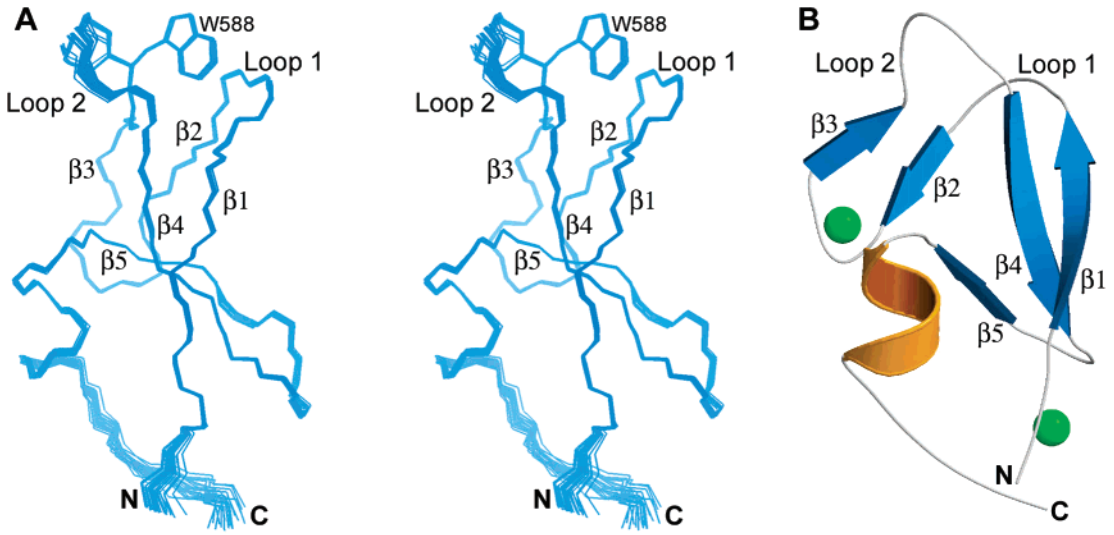

FIGURE 2: Three-dimensional structure in solution of the munc13-1 C_1 domain. (A) Stereodiagram of a backbone superposition of the 20 structures of the munc13-1 C_1 domain with the lowest NOE energies. The side chain of W588 is also shown. (B) Ribbon diagram of a representative structure of the munc13-1 C_1 domain, rotated approximately 50° around the vertical axis with respect to the structures shown in panel A. The β-strands are colored blue and labeled $\beta1-\beta5$; the α-helix is colored orange, and the two Zn^{2+} ions are shown as green spheres. The ligand binding loops are labeled loop 1 and loop 2. N and C indicate the N- and C-termini, respectively. This figure was prepared with Insight II (MSI, San Diego, CA) and Molscript (*36*).

Table 1: Structural Statistics for the 20 Structures of the munc13-1 C_1 Domain with the Lowest NOE Energies[a]

Average rms Deviations from Experimental Restraints (861 total)		
	no.	deviation
NOE distance restraints (Å)		
all	781	0.0065 ± 0.0001
intraresidue	119	0.0052 ± 0.0005
sequential ($\|i-j\|=1$)	164	0.0051 ± 0.0004
short-range ($\|i-j\|=2-4$)	114	0.0086 ± 0.0006
long-range ($\|i-j\|>4$)	384	0.0067 ± 0.0003
hydrogen bonds (Å)	30	0.0058 ± 0.0011
dihedral angles (deg)	50	0.178 ± 0.013
Zn^{2+} binding restraints	18	0.0058 ± 0.0009

Average rms Deviations from Idealized Covalent Geometry	
bonds (Å)	0.0013 ± 0.00004
angles (deg)	0.343 ± 0.004
impropers (deg)	0.163 ± 0.004

Ramachandran Plot Statistics[b]	
residues in most favored regions	73.2%
residues in additionally allowed regions	24.3%
residues in generously allowed regions	1.5%
residues in nonallowed regions	1.0%

Average rms Deviations of Atomic Coordinates (Å)		
	among 20 structures	from the average structure
backbone of residues 567−616	0.38	0.27
heavy atoms of residues 567−616	0.93	0.64
backbone secondary structure[c]	0.14	0.10
heavy atoms secondary structure[c]	0.87	0.60

[a] All 20 structures have NOE energies below 2.8 kcal/mol. There were no NOE violations larger than 0.2 Å or dihedral angle violations larger than 2°. [b] Calculated using PROCHECK (*35*). [c] Residues 569−573, 578−580, 585−587, 593−597, 602−604, and 607−611.

completely different from that observed for the homologous side chain in the PKCδ C_1B domain (W252; see the sequence alignment in Figure 4). Strikingly, the location of the W588 aromatic rings in the munc13-1 C_1 domain practically coincides with the location of two of the rings from the PE bound to the PKCδ C_1B domain (Figure 3B). The interactions of the W588 side chain with the groove between loops 1 and 2 in the munc13-1 C_1 domain mimic in part the interactions that mediate binding of PE to the PKCδ C_1B domain, but there are also some important distinctions.

In the PKCδ C_1B domain, the PE is "sandwiched" between the two loops, making extensive contacts with the backbone atoms of residues Y238−T242 and L251−L254, as well as with the side chains of Y238, P241, L250, and Q257 (see ref *15*). As shown by the space filling model in Figure 3C and the accessible surface representation in Figure 3D, in the munc13-1 C_1 domain the W588 side chain also packs against the backbone atoms of loop 1 (residues A574−P577, which correspond to Y238−P241, respectively, in PKCδ; see Figure 4) and the side chains of A574, P577, and L586 (corresponding to Y238, P241, and L250, respectively, in PKCδ). However, the W588 side chain makes little contact with the backbone of loop 2 because of its different conformation, and instead packs against the side chain of R592 (K256 in PKCδ). Importantly, one ketone and two hydroxyl groups of the PE, which likely mimic the hydroxyl and ester groups of DAG, form one hydrogen bond with the backbone of loop 1 and three hydrogen bonds with the backbone of loop 2 upon binding to the PKCδ C_1B domain (*15*). These hydrogen bonds likely make a substantial contribution to the affinity and specificity of C_1 domains for PEs and DAG, but are not established in the intramolecular interaction involving W588 of the munc13−1 C_1 domain because it lacks these functional groups (note that the aromatic NH group is exposed to the solvent; see panels C and D of Figure 3). Thus, the intramolecular occlusion of the DAG/PE-binding site by W588 in the munc13-1 C_1 domain is expected to decrease ligand affinity but not to prevent ligand binding.

The different structural behavior of the munc13-1 C_1 domain and PKCδ C_1B domain is surprising given the

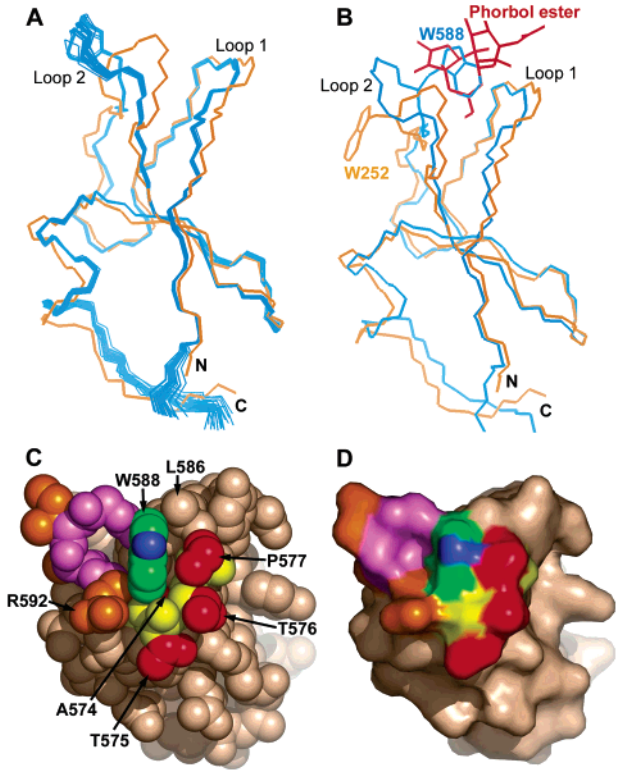

FIGURE 3: The W588 side chain occludes the ligand-binding site of the munc13-1 C_1 domain. (A) Backbone superposition of the 20 NMR structures of the munc13-1 C_1 domain (blue) with the X-ray structure of the apo PKCδ C_1B domain (orange; PDB entry 1PTQ). (B) Backbone superposition of a representative structure of the munc13-1 C_1 domain (blue) with the X-ray structure of the PKCδ C_1B domain (orange) bound to phorbol 13-acetate (red) (PDB entry 1PTR). The side chains of W588 from the munc13-1 C_1 domain and of W252 from the PKCδ C_1B domain are also shown. (C and D) Space filling model (C) and accessible surface (D) of the munc13-1 C_1 domain, viewed from the top of the domain, illustrating how the W588 side chain packs against the rest of the domain. Backbone atoms of loops 1 and 2 are colored yellow and violet, respectively, and side chain atoms from these loops are colored red and orange, respectively, except for those of the W588 side chain, which are colored green (for carbon atoms) and blue (for nitrogen atoms). The positions of some of the side chains are labeled. This figure was prepared with Insight II (MSI) and Pymol (DeLano Scientific, San Carlos, CA).

considerable sequence homology between these C_1 domains (62% of the residues are conserved and 40% of the residues identical) and the fact that the PKCδ C_1B domain also contains a tryptophan in the position homologous to W588 of munc13-1 (Figure 4). Among the four side chains that contact the W588 aromatic ring in the munc13-1 C_1 domain (A574, P577, L586, and R592), only A574 is not identical or conserved in PKCδ. The corresponding PKCδ side chain (Y238) points away from the ligand-binding site, and its β-CH_2 group could establish the same contacts with the W252 side chain that are observed between W588 and A574 in the munc13-1 C_1 domain. Hence, the fact that W588 packs against the ligand-binding site in the munc13-1 C_1 domain but not in the PKCδ C_1B domain appears to arise from differential conformational preferences of the backbone of loops 1 and 2, and perhaps from slight overall structural differences between the two C_1 domains, rather than from contacts between the W588 aromatic ring and specific side chains of the munc13-1 C_1 domain. The alignment of selected DAG/PE-binding C_1 domains shown in Figure 4 (reviewed in ref *3*) illustrates the high level of sequence conservation among the C_1 domains of unc13/munc13 homologues (e.g., 90% of the sequence is identical in the rat munc13-1 and the *Drosophila* unc13 C_1 domains), and the fact that a substantial number of residues are selectively conserved in unc13/munc13 C_1 domains but not in other C_1 domains. Thus, it seems likely that the structural features that determine the intramolecular occlusion of the ligand-binding site by the W588 side chain in the munc13-1 C_1 domain are selectively conserved in the unc13/munc13 family. This proposal is supported by the observation that the homologous aromatic side chains of the PKCα and PKCγ C_1B domains adopt orientations similar to that observed for W252 in the PKCδ C_1B domain (*14*, *18*), but further experimentation will be required to verify this notion for other C_1 domains.

W588 Is Essential for Binding of DAG to the munc13-1 C_1 Domain. Our results indicate that binding of a ligand to the munc13-1 C_1 domain requires a large structural change in loop 2 that removes the W588 side chain from the binding site and leads to the proper backbone conformation for hydrogen bonding to the ligand. To obtain evidence supporting this notion, we acquired $^1H-^{15}N$ HSQC spectra of the munc13-1 C_1 domain in the presence of CHAPS micelles lacking or containing dioctanoylglycerol (DOG). The detergent caused slight shifts in some of the cross-peaks corresponding to amide groups from loops 1 and 2 (data not shown), indicating weak binding of the domain to the micelles that likely arises from the hydrophobicity of this region. Comparison of the spectra obtained in the absence and presence of DOG (Figure 5A, black and red contours, respectively) revealed that DOG binding leads to broadening of a subset of cross-peaks. Some of these cross-peaks were still observable and exhibited significant ligand-induced shifts, while others broadened beyond detection. These observations can be attributed to slow chemical exchange between the ligand-free and ligand-bound domain, which is expected to induce stronger broadening for the amide groups that experience larger chemical shift changes upon ligand binding. Importantly, mapping the ligand-induced cross-peak perturbations on the structure of the munc13-1 C_1 domain (Figure 5B) showed that most of the cross-peaks that broaden beyond detection correspond to amide groups from loop 2 and adjacent residues, which were expected to undergo the largest conformational changes upon ligand binding (see panels A and B of Figure 3). The conformation of loop 1 is expected to be less affected by ligand binding (see panels A and B of Figure 3), but the structural changes in loop 2 and replacement of the W588 side chain with the ligand were also expected to induce significant perturbations in the amide groups of loop 1. Correspondingly, one cross-peak from this loop was also broadened beyond detection, and other cross-peaks from amide groups from this loop and adjacent sequences exhibited significant shifts (Figure 5A,B). It is somewhat surprising that the cross-peak from the indole ring of W588 exhibits only a slight shift upon DOG binding (Figure 5A). However, this indole NH group is highly exposed to the solvent in the structure of both the munc13-1 C_1 domain (Figure 3C,D) and the PKCδ C_1B domain (see Figure 1 of the Supporting Information), and hence, it is plausible that its chemical environment is not highly altered by ligand binding. In addition, the observation of a substantial decrease in the tryptophan fluorescence of the munc13-1 C_1

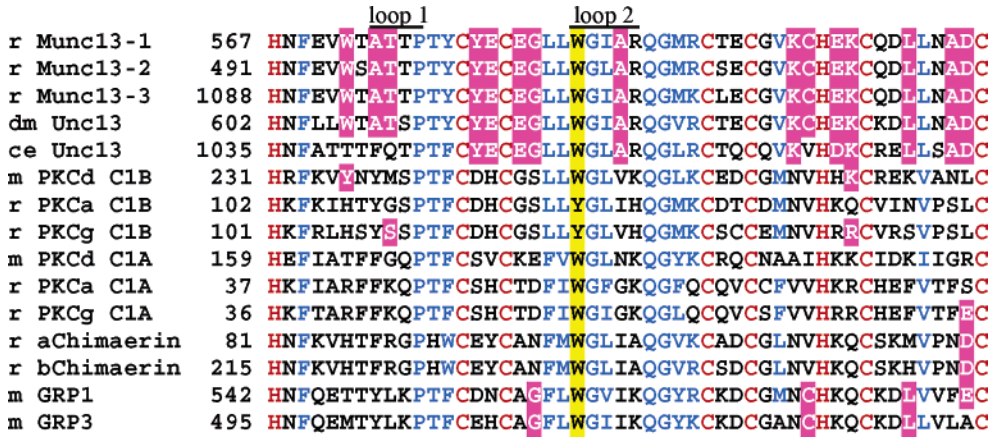

FIGURE 4: Sequence alignment of DAG/PE-binding C_1 domains. Residues involved in Zn^{2+} binding are colored red, and residues in the position homologous to W588 of the munc13-1 C_1 domain are depicted with a yellow background. Other residues that are conserved in at least 80% of the sequences (assuming S = T, E = D, R = K, and L = I = V = F = Y = W) are colored blue. Residues that appear to be selectively conserved in unc13/munc13 C_1 domains are depicted in white with a pink background. The species [r, *Rattus norvegicus*; dm, *Drosophila melanogaster*; ce, *C. elegans*; and m, *Mus musculus* (mouse)] is indicated before the protein name, and the number of the first residue in the sequence is indicated afterward. The Swiss-Prot accession numbers are as follows: Q62768 for r munc13-1, Q62769 for r munc13-2, Q62770 for r munc13-3, Q9U4K9 for dm unc13, P27715 for ce unc13, P28867 for m PKCδ, P05696 for r PKCα, P63319 for r PKCγ, P30337 for r α-chimaerin, Q03070 for r β-chimaerin, Q9Z1S3 for mGRP1, and Q81V61 for mGRP3.

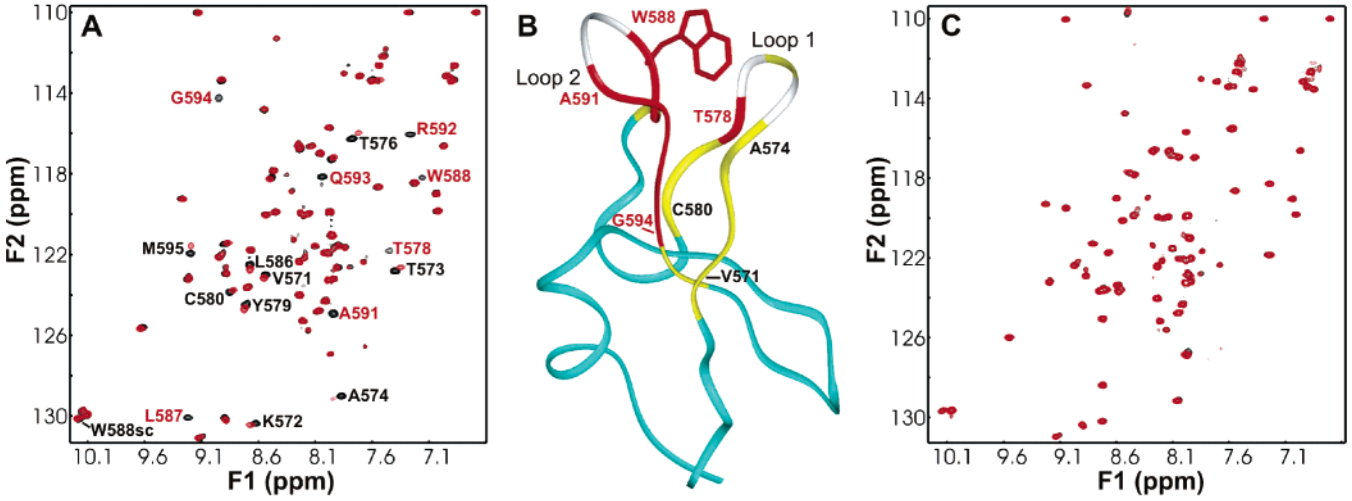

FIGURE 5: DOG binds to the wild-type munc13-1 C_1 domain but not to the W588A mutant. (A) $^1H-^{15}N$ HSQC spectra of the wild-type munc13-1 C_1 domain (100 μM) in 20 mM CHAPS and in the absence (black contours) or presence (red contours) of 0.7 mM DOG. Cross-peaks that broaden beyond detection or exhibit significant shifts upon DOG binding are indicated with red and black labels, respectively. (B) Ribbon diagram of the munc13-1 C_1 domain illustrating the location of the $^1H-^{15}N$ HSQC spectral perturbations induced by DOG. Residues whose NH groups are broadened beyond detection are colored red, and those that exhibit significant cross-peak shifts are colored yellow. The proline residue and residues whose NH groups could not be detected in the absence of DOG are colored white. The positions of some of the residues have been labeled to aid in locating the spectral perturbations observed in panel A. (C) $^1H-^{15}N$ HSQC spectra of the W588A mutant munc13-1 C_1 domain (100 μM) in 20 mM CHAPS and in the absence (black contours) or presence (red contours) of 0.7 mM DOG.

domain upon DOG binding (see Figure 2 of the Supporting Information) provided further evidence for a DOG-induced conformational change involving a tryptophan side chain.

Overall, our results strongly support the notion that binding of a ligand to the munc13-1 C_1 domain requires a conformational change that is not shared by the PKCα, -γ, and -δ C_1B domains, and that appears to depend critically on the W588 side chain. The immediate question that arises is why W588 is conserved in the PKC C_1B domains, where the homologous side chains adopt a completely different orientation, pointing away from the ligand-binding site. In the PKC C_1B domains, this aromatic side chain packs primarily against backbone atoms and a conserved histidine that participates in Zn^{2+} coordination (see Figure 1 of the Supporting Information and refs *14*, *15*, and *18*). These observations suggest that such packing interactions may be critical in stabilizing the structure required for binding of DAG/PE to C_1 domains, which presumably is adopted by the munc13-1 C_1 domain only upon ligand binding. In addition, the hydrophobicity of this side chain is believed to contribute to membrane insertion (*13*, *15*). To test the importance of the W588 side chain for ligand binding to the munc13-1 C_1 domain, we prepared a mutant bearing a point Trp588 to Ala substitution (W588A mutant) and tested for DOG binding using $^1H-^{15}N$ HSQC spectra. The spectra did not reveal any significant DOG-induced cross-peak shifts (Figure 5), showing that the mutant does not bind DOG even at the high protein and ligand concentrations used in these experiments. These results strongly support the notion that the W588 side chain of the munc13-1 C_1 domain plays a dual

role, occluding the binding site in the apo structure and stabilizing the holo structure upon ligand binding.

DISCUSSION

DAG acts as a second messenger in a wide variety of signaling pathways that naturally involve a diversity of DAG receptors. The numerous isoforms of PKC account in part for this diversity, but it is now clear that several non-PKC receptors such as unc13/munc13s mediate some key DAG-dependent signaling processes. Indeed, the functional importance of munc13-1 as a DAG receptor is underlined by the lethal phenotype caused by mutations in its C_1 domain (*12*). Whereas the published structures of several PKC C_1 domains had revealed the overall architecture of these DAG/PE-binding domains and the structural basis for PE binding, it was unknown whether the C_1 domains of alternative DAG receptors contain specific structural features that might underlie important functional distinctions. The structure of the munc13-1 C_1 domain described here constitutes the first reported structure of a C_1 domain from a non-PKC target of DAG signaling and uncovers an unexpected structural difference with the PKC C_1 domains, the occlusion of the DAG/PE-binding site by a conserved tryptophan side chain that is at the same time critical for ligand binding. The high level of sequence conservation of C_1 domains in unc13/munc13 homologues (Figure 4) suggests that such an occlusion is conserved in this protein family and that this structural feature may be crucial for how unc13/munc13s mediate augmentation of neurotransmitter release by DAG.

The obvious functional consequence that can be expected from the occlusion of the ligand-binding site by the W588 side chain of the munc13-1 C_1 domain is a lower binding affinity for DAG compared to the affinities of C_1 domains that do not share this feature such as those of PKCs, since binding of a ligand to the former C_1 domain requires shifting the equilibrium between ligand-free and ligand-bound conformations. The phorbol binding affinity reported for the munc13-1 C_1 domain [$k_D = 5$ nM (*30*)] indeed appears to be somewhat lower than those reported for PKC C_1 domains under similar conditions [k_D values from 0.5 nM to low nanomolar (*31*, *32*)]. These differences were not considered significant given the variability in the k_D values measured for PKC, but they suggest that the ligand affinity of the munc13-1 C_1 domain could be up to 10-fold lower than those of the PKC C_1 domains. Indeed, these differences could be even larger, since it is very difficult to accurately measure these dissociation constants because of the high affinities involved, their dependence on diverse factors such as the amount of phosphatidylserine present in the micelles or vesicles used in these experiments, and the highly hydrophobic nature of the ligands (see, for instance, refs *32* and *33*). In addition, kinetic factors may be critical determinants of the levels of DAG required for receptor activation in vivo, since increases in DAG concentration induced by a signal may be temporarily localized to specific sites of the membrane and quickly decrease by lateral diffusion. The occlusion of the DAG-binding site observed in the structure of the munc13-1 C_1 domain is expected to impose a kinetic barrier for ligand binding and hence decrease the binding on rate. Combined with a gradually decreasing DAG concentration at the site of action, a slower on rate would also result in munc13-1 activation at DAG levels higher than those required by receptors whose C_1 domain does not exhibit occlusion of the DAG-binding site. These arguments lead us to hypothesize that munc13-1-dependent augmentation of neurotransmitter release is activated at higher DAG levels than PKCs.

What purpose could a response by munc13-1 at a DAG threshold higher than that of PKCs serve? Discrimination of the multitude of DAG-dependent signals by distinct types of DAG receptors poses a complex biological problem reminiscent of the need for different Ca^{2+} receptors to respond to distinct Ca^{2+}-mediated signals. For instance, neurotransmitter release is tightly regulated by the influx of extracellular Ca^{2+} when an action potential reaches a presynaptic terminal, and it would be highly undesirable if release would be triggered by the multitude of unrelated signaling processes that are controlled by changes in intracellular Ca^{2+} concentration. The selective response of the release machinery to action potentials relies on the use of a low-affinity Ca^{2+} sensor, synaptotagmin 1 (*34*), which only responds to the temporarily very high Ca^{2+} concentrations existing near the Ca^{2+} channels that are opened by action potentials. Similarly, it seems likely that DAG-mediated augmentation of neurotransmitter release needs to be uncoupled from the multitude of other regulatory processes that depend on DAG. Our hypothesis that munc13-1 is activated at higher DAG levels than PKCs provides an attractive mechanism for achieving such uncoupling that would parallel the selective activation of neurotransmitter release at high Ca^{2+} concentrations. Although alternative mechanisms for distinguishing between different types of DAG signals can be envisaged and studies in living cells will be required to test our hypothesis, our results provide a nice illustration of how even highly homologous domains may exhibit striking structural differences and how discovery of such differences can open novel ideas about key biological processes.

SUPPORTING INFORMATION AVAILABLE

Space filling model and accessible surface of the apo PKCδ C_1B domain (Figure 1) and DOG binding induces changes in the tryptophan fluorescence of the munc13-1 C_1 domain (Figure 2). This material is available free of charge via the Internet at http://pubs.acs.org.

REFERENCES

1. Nishizuka, Y. (1995) Protein kinase C and lipid signaling for sustained cellular responses, *FASEB J. 9*, 484−496.
2. Newton, A. C. (1995) Protein kinase C: Structure, function, and regulation, *J. Biol. Chem. 270*, 28495−28498.
3. Kazanietz, M. G. (2002) Novel "nonkinase" phorbol ester receptors: The C1 domain connection, *Mol. Pharmacol. 61*, 759−767.
4. Brose, N., and Rosenmund, C. (2002) Move over protein kinase C, you've got company: Alternative cellular effectors of diacylglycerol and phorbol esters, *J. Cell Sci. 115*, 4399−4411.
5. Silinsky, E. M., and Searl, T. J. (2003) Phorbol esters and neurotransmitter release: More than just protein kinase C? *Br. J. Pharmacol. 138*, 1191−1201.
6. Brose, N., Rosenmund, C., and Rettig, J. (2000) Regulation of transmitter release by Unc-13 and its homologues, *Curr. Opin. Neurobiol. 10*, 303−311.
7. Augustin, I., Rosenmund, C., Sudhof, T. C., and Brose, N. (1999) Munc13-1 is essential for fusion competence of glutamatergic synaptic vesicles, *Nature 400*, 457−461.
8. Varoqueaux, F., Sigler, A., Rhee, J. S., Brose, N., Enk, C., Reim, K., and Rosenmund, C. (2002) Total arrest of spontaneous and evoked synaptic transmission but normal synaptogenesis in the

absence of Munc13-mediated vesicle priming, *Proc. Natl. Acad. Sci. U.S.A. 99*, 9037−9042.
9. Richmond, J. E., Davis, W. S., and Jorgensen, E. M. (1999) UNC-13 is required for synaptic vesicle fusion in *C. elegans*, *Nat. Neurosci. 2*, 959−964.
10. Aravamudan, B., Fergestad, T., Davis, W. S., Rodesch, C. K., and Broadie, K. (1999) Drosophila UNC-13 is essential for synaptic transmission, *Nat. Neurosci. 2*, 965−971.
11. Lackner, M. R., Nurrish, S. J., and Kaplan, J. M. (1999) Facilitation of synaptic transmission by EGL-30 Gqα and EGL-8 PLCβ: DAG binding to UNC-13 is required to stimulate acetylcholine release, *Neuron 24*, 335−346.
12. Rhee, J. S., Betz, A., Pyott, S., Reim, K., Varoqueaux, F., Augustin, I., Hesse, D., Sudhof, T. C., Takahashi, M., Rosenmund, C., and Brose, N. (2002) β-Phorbol ester- and diacylglycerol-induced augmentation of transmitter release is mediated by Munc13s and not by PKCs, *Cell 108*, 121−133.
13. Hurley, J. H., Newton, A. C., Parker, P. J., Blumberg, P. M., and Nishizuka, Y. (1997) Taxonomy and function of C1 protein kinase C homology domains, *Protein Sci. 6*, 477−480.
14. Hommel, U., Zurini, M., and Luyten, M. (1994) Solution structure of a cysteine rich domain of rat protein kinase C, *Nat. Struct. Biol. 1*, 383−387.
15. Zhang, G., Kazanietz, M. G., Blumberg, P. M., and Hurley, J. H. (1995) Crystal structure of the Cys2 activator-binding domain of protein kinase C δ in complex with phorbol ester, *Cell 81*, 917−924.
16. Mott, H. R., Carpenter, J. W., Zhong, S., Ghosh, S., Bell, R. M., and Campbell, S. L. (1996) The solution structure of the Raf-1 cysteine-rich domain: A novel ras and phospholipid binding site, *Proc. Natl. Acad. Sci. U.S.A. 93*, 8312−8317.
17. Zhou, M., Horita, D. A., Waugh, D. S., Byrd, R. A., and Morrison, D. K. (2002) Solution structure and functional analysis of the cysteine-rich C1 domain of kinase suppressor of Ras (KSR), *J. Mol. Biol. 315*, 435−446.
18. Xu, R. X., Pawelczyk, T., Xia, T. H., and Brown, S. C. (1997) NMR structure of a protein kinase C-γ phorbol-binding domain and study of protein−lipid micelle interactions, *Biochemistry 36*, 10709−10717.
19. Brose, N., Hofmann, K., Hata, Y., and Sudhof, T. C. (1995) Mammalian homologues of *Caenorhabditis elegans* unc-13 gene define novel family of C2-domain proteins, *J. Biol. Chem. 270*, 25273−25280.
20. Guan, K. L., and Dixon, J. E. (1991) Eukaryotic proteins expressed in *Escherichia coli*: An improved thrombin cleavage and purification procedure of fusion proteins with glutathione *S*-transferase, *Anal. Biochem. 192*, 262−267.
21. Kay, L. E., Xu, G. Y., Singer, A. U., Muhandiram, D. R., and Formankay, J. D. (1993) A Gradient-Enhanced HCCH Tocsy Experiment for Recording Side-Chain H-1 and C-13 Correlations in H_2O Samples of Proteins, *J. Magn. Reson., Ser. B 101*, 333−337.
22. Kay, L. E., Xu, G. Y., and Yamazaki, T. (1994) Enhanced-Sensitivity Triple-Resonance Spectroscopy with Minimal H_2O Saturation, *J. Magn. Reson., Ser. A 109*, 129−133.
23. Muhandiram, D. R., and Kay, L. E. (1994) Gradient-Enhanced Triple-Resonance 3-Dimensional NMR Experiments with Improved Sensitivity, *J. Magn. Reson., Ser. B 103*, 203−216.
24. Bax, A., Max, D., and Zax, D. (1992) Measurement of Long-Range $^{13}C-^{13}C$ *J* Couplings in a 20-kDa Protein−Peptide Complex, *J. Am. Chem. Soc. 114*, 6923−6925.
25. Delaglio, F., Grzesiek, S., Vuister, G. W., Zhu, G., Pfeifer, J., and Bax, A. (1995) Nmrpipe: A Multidimensional Spectral Processing System Based on Unix Pipes, *J. Biomol. NMR 6*, 277−293.
26. Johnson, B. A., and Blevins, R. A. (1994) NMR View: A Computer-Program for the Visualization and Analysis of NMR Data, *J. Biomol. NMR 4*, 603−614.
27. Cornilescu, G., Delaglio, F., and Bax, A. (1999) Protein backbone angle restraints from searching a database for chemical shift and sequence homology, *J. Biomol. NMR 13*, 289−302.
28. Brunger, A. T., Adams, P. D., Clore, G. M., DeLano, W. L., Gros, P., Grosse-Kunstleve, R. W., Jiang, J. S., Kuszewski, J., Nilges, M., Pannu, N. S., Read, R. J., Rice, L. M., Simonson, T., and Warren, G. L. (1998) Crystallography & NMR system: A new software suite for macromolecular structure determination, *Acta Crystallogr. D54* (Part 5), 905−921.
29. Holm, L., and Sander, C. (1993) Protein structure comparison by alignment of distance matrices, *J. Mol. Biol. 233*, 123−138.
30. Betz, A., Ashery, U., Rickmann, M., Augustin, I., Neher, E., Sudhof, T. C., Rettig, J., and Brose, N. (1998) Munc13-1 is a presynaptic phorbol ester receptor that enhances neurotransmitter release, *Neuron 21*, 123−136.
31. Wang, Q. J., Fang, T. W., Nacro, K., Marquez, V. E., Wang, S., and Blumberg, P. M. (2001) Role of hydrophobic residues in the C1b domain of protein kinase C δ on ligand and phospholipid interactions, *J. Biol. Chem. 276*, 19580−19587.
32. Ananthanarayanan, B., Stahelin, R. V., Digman, M. A., and Cho, W. (2003) Activation mechanisms of conventional protein kinase C isoforms are determined by the ligand affinity and conformational flexibility of their C1 domains, *J. Biol. Chem. 278*, 46886−46894.
33. Sharkey, N. A., and Blumberg, P. M. (1985) Highly lipophilic phorbol esters as inhibitors of specific [^{3}H]phorbol 12,13-dibutyrate binding, *Cancer Res. 45*, 19−24.
34. Fernandez-Chacon, R., Konigstorfer, A., Gerber, S. H., Garcia, J., Matos, M. F., Stevens, C. F., Brose, N., Rizo, J., Rosenmund, C., and Sudhof, T. C. (2001) Synaptotagmin I functions as a calcium regulator of release probability, *Nature 410*, 41−49.
35. Laskowski, R. A., Macarthur, M. W., Moss, D. S., and Thornton, J. M. (1993) Procheck: A Program to Check the Stereochemical Quality of Protein Structures, *J. Appl. Crystallogr. 26*, 283−291.
36. Kraulis, P. J. (1991) Molscript: A Program to Produce Both Detailed and Schematic Plots of Protein Structures, *J. Appl. Crystallogr. 24*, 946−950.

BI0476127